Reprinted from "Scattering and Surface Roughness," Z.-H. Gu and A. A. Maradudin, Editors, Proc. SPIE 3141, 220-231 (1997)

A goniometric optical scatter instrument for bidirectional reflectance distribution function measurements with out-of-plane and polarimetry capabilities

Thomas A. Germer and Clara C. Asmail

Optical Technology Division
National Institute of Standards and Technology
Gaithersburg, Maryland 20899

ABSTRACT

A goniometric optical scatter instrument has been developed at the National Institute of Standards and Technology which can readily perform out-of-plane measurements of optical scatter as well as polarimetric measurements. This paper uses the description of this instrument as a platform to discuss key issues that must be addressed when developing either out-of-plane measurement capabilities or polarimetric capabilities, or both at the same time. The transformation from the sample coordinates to the instrument coordinates has been carried out, including the rotation of the polarization coordinates for out-of-plane measurements. The out-of-plane instrument signature that results from Rayleigh scatter in air is calculated and compared with measurement. Finally, the results of some out-of-plane Mueller matrix BRDF measurements of the backside of a silicon wafer are presented.

Keywords: goniometer, BRDF, polarimetry

1. INTRODUCTION

Optical scattering has been shown to be a powerful diagnostic technique for characterizing optical quality surfaces.[1] The fundamental description of optical scattering can be encapsulated in the bidirectional reflectance distribution function (BRDF), defined as the scattered radiance normalized by the incident irradiance, given by

$$f(\theta_\mathrm{i}, \phi_\mathrm{i}; \theta_\mathrm{s}, \phi_\mathrm{s}) = \frac{\partial \Phi_\mathrm{s}}{\partial \omega} \frac{1}{\Phi_\mathrm{i} \cos \theta_\mathrm{s}}, \tag{1}$$

where $\partial\Phi_\mathrm{s}/\partial\omega$ is the scattered power per unit solid angle, Φ_i is the incident power, θ_s is the scattering polar angle, ϕ_s is the scattering azimuthal angle, θ_i is the incident polar angle, and ϕ_i is the incident azimuthal angle, as illustrated in Fig. 1. Although the BRDF is often reported as a polarization-averaged quantity, it should in fact be a Mueller matrix, relating the scattered polarization state to the incident polarization state. Calculations, and recent experimental results, have demonstrated that a wealth of information is included in the polarimetric properties of many samples.[2–11] Even more so, the polarimetric properties of scattering out of the plane of incidence can allow making distinctions among different types of defects.[5,6]

The Goniometric Optical Scatter Instrument (GOSI) has been described in a previous publication.[12] This article will elaborate on issues which are specific to performing polarimetric measurements out of the plane of incidence, and describe modifications which have been made to the instrument since the previously described work.

Section 2 will describe the instrument. In Sec. 3, the algorithms for converting between the goniometer angles and the sample coordinate system will be derived. In Sec. 4, the instrument signature that arises due to Rayleigh scattering in the air surrounding the sample will be derived, and the results compared to experiment. Finally, in Sec. 5, some experimental results of out-of-plane Mueller matrix measurements will be presented.

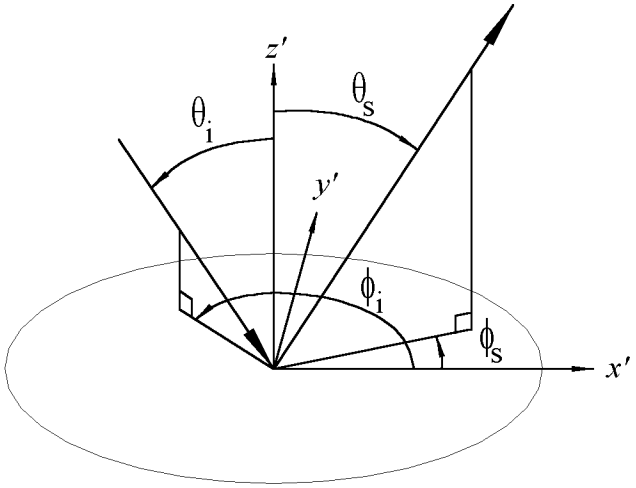

Figure 1 The sample coordinate system.

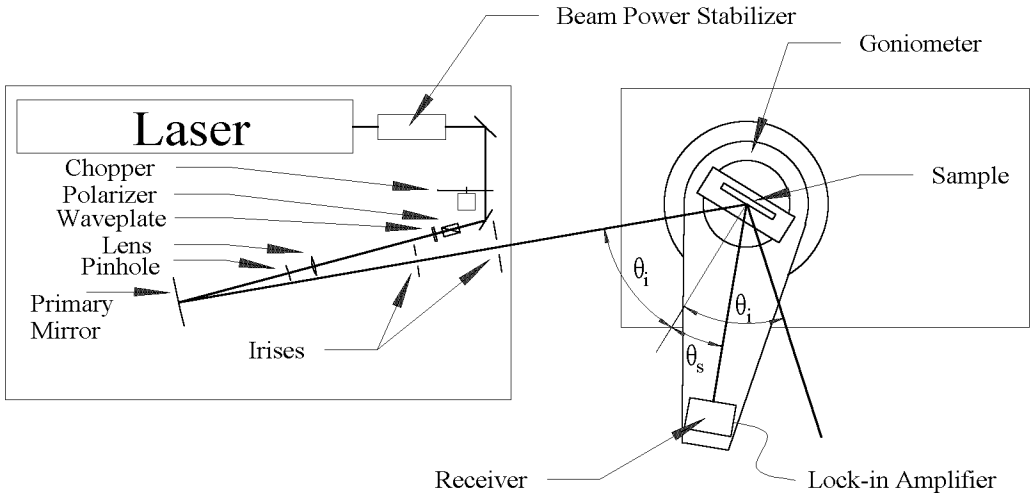

Figure 2 An overall schematic of the Goniometric Optical Scatter Instrument (GOSI). The angles θ_{i} and θ_{s} are shown for the case of the sample normal lying in the plane of the page. (Not to scale.)

2. DESCRIPTION OF THE INSTRUMENT

Figure 2 shows an overall schematic diagram of GOSI. Light from one of three lasers, HeNe (633 nm), frequency-doubled Nd:YAG (532 nm), and HeCd (442 nm or 325 nm), passes through a power stabilizer, a chopper, a polarizer, a retarder (currently $\lambda/2$) mounted on a computer controlled rotation stage, a lens, and a pinhole before being directed and focussed with a super-polished concave mirror through the center of a goniometer. The light is focused to the angle-defining aperture of a receiver.

Figure 3 shows a schematic diagram of the goniometer. It is a three-axis four-angle goniometer with α being the angle of rotation of the sample about a vertical axis, β being the angle of rotation of the sample about a horizontal axis which moves with α, γ being an angle of rotation about the sample azimuth (moving with α and β), and δ being the angle of rotation of the detector about the vertical axis. When $\alpha = \beta = \gamma = \delta = 0$, the sample is positioned so that the light is at normal incidence and the detector (if it were not blocking the incident light) is positioned to collect the specularly reflected light ($\theta_{\mathrm{i}} = \theta_{\mathrm{s}} = 0$). With this configuration nearly any combination of incident and scattering directions can be achieved, being limited only by obscuration of either the incident

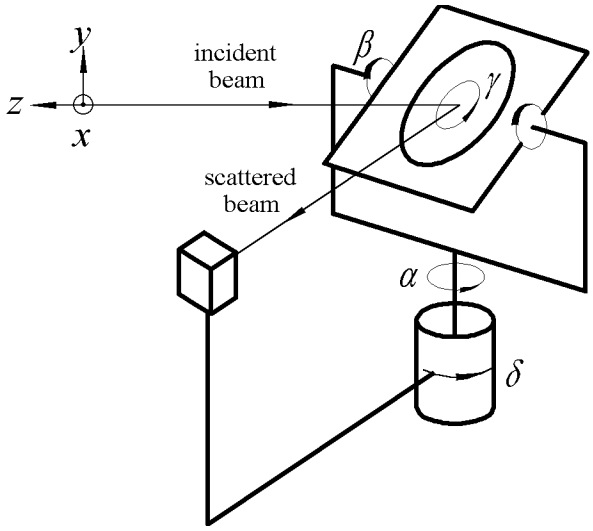

Figure 3 A schematic diagram of GOSI's goniometer. The angle γ represents a rotation about the sample normal.

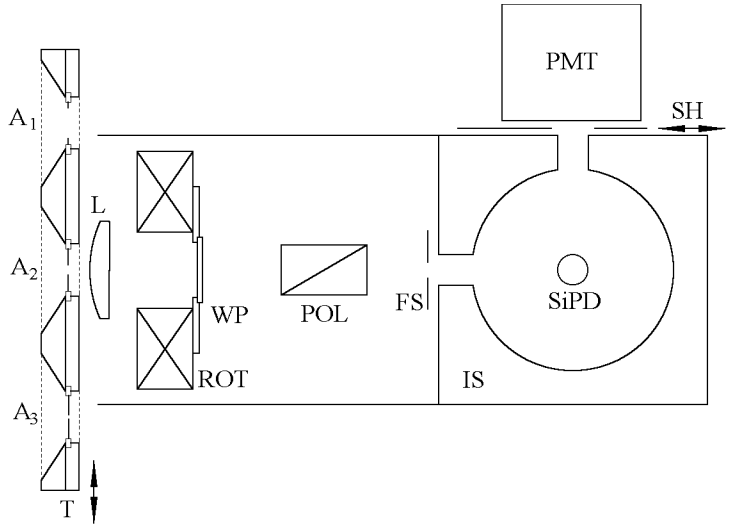

Figure 4 A schematic of the instrument's receiver (not to scale): A_1, A_2, and A_3 are solid-angle-limiting apertures, mounted on a translation stage T; L is a lens; WP is a $\lambda/2$ retarder, mounted on a rotation stage ROT; POL is a polarizer; FS is an adjustable iris field stop; IS is an integrating sphere; PMT is a photomultiplier tube; SH is a manual shutter; and SiPD is a silicon photodiode.

or scattered beam by the sample mount (at angles $\theta > 87°$) or occultation of the incident beam by the receiver (within 5° of retroreflection).

Figure 4 shows a schematic of the receiver. A computer-controlled translation stage selects one of three collection-solid-angle-limiting apertures ($A_1 = 1.17 \times 10^{-4}$ sr, $A_2 = 2.39 \times 10^{-6}$ sr, and $A_3 = 9.6 \times 10^{-8}$ sr) to optimize required angular sensitivity or collection efficiency. A lens (L) is positioned behind the apertures to focus the sample plane onto an adjustable iris field stop (FS). A linear retarder (WP) (currently $\lambda/2$) is mounted onto a computer controlled rotation stage (ROT). A Glan-Thompson polarizer (POL) mounted onto a manual rotary stage follows the retarder; during measurements, the polarizer is maintained fixed. After passing through the field stop, the light is collected in an integrating sphere (IS). The lens, retarder, polarizer, and adjustable field

stop are enhancements to the current design which differ from the previous publication. The integrating sphere has two ports, onto which two detectors, a silicon photodiode (SiPD) and a photomultiplier tube (PMT), are mounted. The PMT has a manual shutter to prevent exposure to excessive light levels. The signal from either the photodiode or the PMT is recorded by a lock-in amplifier. This receiver design has a linear dynamic range of about 15 orders of magnitude (in units of sr^{-1}), a minimum angular resolution of 0.02°, and a polarization extinction factor of about 10^4. The instrument signature is Rayleigh-scattering-limited within about 1° from the specular direction.[12,13]

3. TRANSFORMATIONS

A. Converting Goniometer Angles to Sample Reference Frame Angles

The sample reference frame coordinate system is shown in Fig. 1. It is the purpose of this section to derive the expressions necessary to convert the goniometer angles α, β, γ, and δ to the sample coordinate system angles θ_i, ϕ_i, θ_s, and ϕ_s. In Sec. 3.B, the transformation will be inverted.

We begin by defining a coordinate system using the basis vectors $\{\hat{\mathbf{x}}, \hat{\mathbf{y}}, \hat{\mathbf{z}}\}$ which is fixed with respect to the laboratory. We then introduce the rotation matrix

$$R_\mathrm{samp}(\alpha, \beta, \gamma) = R(\hat{\mathbf{y}}, \alpha) R(\hat{\mathbf{x}}, \beta) R(\hat{\mathbf{z}}, \gamma), \tag{2}$$

where $R(\hat{\mathbf{v}}, \theta)$ is the matrix which rotates the coordinate system an angle θ clockwise about the vector $\hat{\mathbf{v}}$. The matrix R_samp, when acting upon a vector fixed with respect to the sample, first rotates it an angle γ about $\hat{\mathbf{z}}$, then an angle β about $\hat{\mathbf{x}}$, and finally an angle α about $\hat{\mathbf{y}}$. Written explicitly, this matrix is

$$R_\mathrm{samp}(\alpha, \beta, \gamma) = \begin{pmatrix} \cos\alpha\,\cos\gamma - \sin\alpha\,\sin\beta\,\sin\gamma & \cos\gamma\,\sin\alpha\,\sin\beta + \cos\alpha\,\sin\gamma & \cos\beta\,\sin\alpha \\ -\cos\beta\,\sin\gamma & \cos\beta\,\cos\gamma & -\sin\beta \\ -\cos\gamma\,\sin\alpha - \cos\alpha\,\sin\beta\,\sin\gamma & \cos\alpha\,\cos\gamma\,\sin\beta - \sin\alpha\,\sin\gamma & \cos\alpha\,\cos\beta \end{pmatrix} \tag{3}$$

When $\alpha = 0$, $\beta = 0$, and $\gamma = 0$, the sample is oriented such that the surface normal is in the $\hat{\mathbf{z}}$ direction. The incoming propagation direction is

$$\hat{\mathbf{k}}_\mathrm{i} = -\hat{\mathbf{z}}, \tag{4}$$

while for an arbitrary δ the detection direction is given by

$$\hat{\mathbf{k}}_\mathrm{s} = R(\hat{\mathbf{y}}, \delta)\hat{\mathbf{z}} = \sin\delta\hat{\mathbf{x}} + \cos\delta\hat{\mathbf{z}}. \tag{5}$$

It is useful to define a new coordinate system fixed with respect to the sample such that for every $\hat{\mathbf{r}} \in \{\hat{\mathbf{x}}, \hat{\mathbf{y}}, \hat{\mathbf{z}}\}$ and $\hat{\mathbf{r}}' \in \{\hat{\mathbf{x}}', \hat{\mathbf{y}}', \hat{\mathbf{z}}'\}$, $\hat{\mathbf{r}}' = R_\mathrm{samp}\hat{\mathbf{r}}$:

$$\hat{\mathbf{x}}' = [\cos\alpha\,\cos\gamma - \sin\alpha\,\sin\beta\,\sin\gamma]\hat{\mathbf{x}} - \cos\beta\,\sin\gamma\hat{\mathbf{y}} - [\cos\gamma\,\sin\alpha + \cos\alpha\,\sin\beta\,\sin\gamma]\hat{\mathbf{z}}, \tag{6}$$

$$\hat{\mathbf{y}}' = [\cos\gamma\,\sin\alpha\,\sin\beta + \cos\alpha\,\sin\gamma]\hat{\mathbf{x}} + \cos\beta\,\cos\gamma\hat{\mathbf{y}} + [\cos\alpha\,\cos\gamma\,\sin\beta - \sin\alpha\,\sin\gamma]\hat{\mathbf{z}}, \tag{7}$$

and

$$\hat{\mathbf{z}}' = \cos\beta\sin\alpha\hat{\mathbf{x}} - \sin\beta\hat{\mathbf{y}} + \cos\alpha\,\cos\beta\hat{\mathbf{z}}. \tag{8}$$

The primed coordinate system tracks the sample orientation in terms of the laboratory-based coordinate system.

It is now straightforward to determine the polar and azimuthal angles of the incoming and outgoing light. The polar angles θ_i and θ_s can be determined from the inner products of $-\hat{\mathbf{k}}_\mathrm{i}$ and $\hat{\mathbf{k}}_\mathrm{s}$ with the surface normal $\hat{\mathbf{z}}'$, respectively:

$$\cos\theta_\mathrm{i} = -\hat{\mathbf{k}}_\mathrm{i} \cdot \hat{\mathbf{z}}' = \cos\alpha\,\cos\beta \tag{9}$$

and

$$\cos\theta_s = \hat{\mathbf{k}}_s \cdot \hat{\mathbf{z}}' = \cos\beta\,\sin\alpha\,\sin\delta + \cos\alpha\,\cos\beta\,\cos\delta. \tag{10}$$

For the azimuthal angles, ϕ_i and ϕ_s, we need the projections of $\hat{\mathbf{k}}_i$ and $\hat{\mathbf{k}}_s$ onto $\hat{\mathbf{x}}'$ and $\hat{\mathbf{y}}'$,

$$\begin{aligned}\phi_i &= \arctan(-\hat{\mathbf{k}}_i \cdot \hat{\mathbf{x}}', -\hat{\mathbf{k}}_i \cdot \hat{\mathbf{y}}') \\ &= \arctan(-\cos\gamma\sin\alpha - \cos\alpha\sin\beta\sin\gamma, \cos\alpha\cos\gamma\sin\beta - \sin\alpha\sin\gamma),\end{aligned} \tag{11}$$

and

$$\begin{aligned}\phi_s &= \arctan(\hat{\mathbf{k}}_s \cdot \hat{\mathbf{x}}', \hat{\mathbf{k}}_s \cdot \hat{\mathbf{y}}') \\ &= \arctan[-\cos\delta\,(\cos\gamma\,\sin\alpha - \cos\alpha\,\sin\beta\,\sin\gamma) + \sin\delta\,(\cos\alpha\,\cos\gamma - \sin\alpha\,\sin\beta\,\sin\gamma)\,, \\ &\qquad \sin\delta\,(\cos\gamma\,\sin\alpha\,\sin\beta + \cos\alpha\,\sin\gamma) + \cos\delta\,(\cos\alpha\,\cos\gamma\,\sin\beta - \sin\alpha\,\sin\gamma)],\end{aligned} \tag{12}$$

where the function $\arctan(x, y)$ gives the polar angle of (x, y):

$$\arctan(x,y) = \left\{ \begin{array}{cc} \arctan(y/x) & \text{if } x > 0 \\ \pi + \arctan(-y/x) & \text{if } x < 0 \\ \pi/2 & \text{if } x = 0 \text{ and } y > 0 \\ -\pi/2 & \text{if } x = 0 \text{ and } y < 0 \end{array} \right\} \tag{13}$$

B. Converting Sample Reference Frame Angles to Goniometer Angles

In Sec. 3.A, we have calculated the sample-relative scattering angles when the goniometer angles are known. However, it is often common to ask the opposite question, and inversion of the results of the last section can be tricky. In this section, we obtain the goniometer angles corresponding to the desired incident and scattering directions, defined by θ_i, ϕ_i, θ_s, and ϕ_s. Since δ is the angle made by the incoming and outgoing beams, we can readily solve for it. Working in a coordinate system convenient to the sample it is apparent from the standard formulae for polar-rectilinear transformations that

$$-\hat{\mathbf{k}}_i = \sin\theta_i\cos\phi_i\hat{\mathbf{x}}' + \sin\theta_i\sin\phi_i\hat{\mathbf{y}}' + \cos\theta_i\hat{\mathbf{z}}' \tag{14}$$

and

$$\hat{\mathbf{k}}_s = \sin\theta_s\cos\phi_s\hat{\mathbf{x}}' + \sin\theta_s\sin\phi_s\hat{\mathbf{y}}' + \cos\theta_s\hat{\mathbf{z}}'. \tag{15}$$

Again, we use the dot product to calculate the cosine of the subtended angle,

$$\begin{aligned}\cos\delta &= \hat{\mathbf{k}}_i \cdot \hat{\mathbf{k}}_s \\ &= \cos\theta_i\cos\theta_s + \cos\phi_i\cos\phi_s\sin\theta_i\sin\theta_s + \sin\phi_i\sin\phi_s\sin\theta_i\sin\theta_s.\end{aligned} \tag{16}$$

Eq. 9 allows us to eliminate β from Eq. 10 and solve for the rotation of the sample about the vertical axis of the goniometer, α:

$$\alpha = \arctan\left(\frac{\cos\theta_s - \cos\theta_i\cos\delta}{\cos\theta_i\sin\delta}\right). \tag{17}$$

By recognizing that

$$\hat{\mathbf{y}} = \frac{-\hat{\mathbf{k}} \times \hat{\mathbf{k}}_s}{|\hat{\mathbf{k}} \times \hat{\mathbf{k}}_s|} \tag{18}$$

is a unit vector pointing in the vertical direction in the laboratory, and $\hat{\mathbf{z}}'$ is the surface normal, β can be derived from

$$\begin{aligned}\sin\beta &= \frac{-\hat{\mathbf{k}}_i \times \hat{\mathbf{k}}_s}{|\hat{\mathbf{k}}_i \times \hat{\mathbf{k}}_s|} \cdot \hat{\mathbf{z}}' \\ &= \sin(\phi_s - \phi_i)\sin\theta_s\sin\theta_i/\sin\delta,\end{aligned} \tag{19}$$

where we have used $\sin\delta = |\hat{\mathbf{k}}_\mathrm{i} \times \hat{\mathbf{k}}_\mathrm{s}|$.

The easiest way to solve for the rotation of the sample about its normal, γ, is to calculate ϕ_i' or ϕ_s' for $\gamma = 0$, using Eqs. 11 and 12, and then set $\gamma = \phi_\mathrm{s} - \phi_\mathrm{s}' = \phi_\mathrm{i} - \phi_\mathrm{i}'$. Therefore,

$$\gamma = \phi_\mathrm{s} - \arctan(-\cos\delta\sin\alpha + \sin\delta\cos\alpha, \sin\delta\sin\alpha\sin\beta + \cos\delta\cos\alpha), \tag{20}$$

where the function $\arctan(x, y)$ is treated as in Eq. 13.

The expressions above lead to intermediate singularities when $\delta = 0$ (retroreflection), for which $\alpha = \theta_\mathrm{i}$ and $\beta = 0$. Also, roundoff errors can lead to problems during in-plane measurements, when $\cos\beta = 1$; values of $\cos\beta > 1$ should return $\beta = 0$.

C. The Polarization Coordinates

We will work under the assumption that the most natural basis vector set for studying the polarization of scattered light is the $\hat{\mathbf{p}}'$ and $\hat{\mathbf{s}}'$ vectors associated with the plane of incidence for the incident light and the plane of exitance for the exiting light. The planes of incidence and exitance are defined by the sample normal and $\hat{\mathbf{k}}_\mathrm{i}$ and $\hat{\mathbf{k}}_\mathrm{s}$, respectively. The basis vectors used to describe the polarization that are most convenient in the laboratory frame are

$$\hat{\mathbf{s}}_\mathrm{i} = \hat{\mathbf{y}}, \tag{21}$$

$$\hat{\mathbf{p}}_\mathrm{i} = \hat{\mathbf{x}}, \tag{22}$$

$$\hat{\mathbf{s}}_\mathrm{s} = \cos\delta\hat{\mathbf{y}} + \sin\delta\hat{\mathbf{z}}, \tag{23}$$

and

$$\hat{\mathbf{p}}_\mathrm{s} = -\hat{\mathbf{x}}. \tag{24}$$

When measuring the polarization properties of out-of-plane optical scattering, we must be aware that the incoming and outgoing polarization analyzers must be rotated so that they remain in the sample coordinate system. Therefore, we define a set of basis vectors

$$\hat{\mathbf{s}}_\mathrm{i}' = \frac{\hat{\mathbf{k}}_\mathrm{i} \times \hat{\mathbf{z}}'}{|\hat{\mathbf{k}}_\mathrm{i} \times \hat{\mathbf{z}}'|}, \tag{25}$$

$$\hat{\mathbf{p}}_\mathrm{i}' = \hat{\mathbf{k}}_\mathrm{i} \times \hat{\mathbf{s}}_\mathrm{i}, \tag{26}$$

$$\hat{\mathbf{s}}_\mathrm{s}' = \frac{\hat{\mathbf{k}}_\mathrm{s} \times \hat{\mathbf{z}}'}{|\hat{\mathbf{k}}_\mathrm{s} \times \hat{\mathbf{z}}'|}, \tag{27}$$

and

$$\hat{\mathbf{p}}_\mathrm{s}' = \hat{\mathbf{k}}_\mathrm{s} \times \hat{\mathbf{s}}_\mathrm{s}. \tag{28}$$

It can be verified that the four sets of unit vectors, $\{\hat{\mathbf{s}}_\mathrm{i}, \hat{\mathbf{p}}_\mathrm{i}, \hat{\mathbf{k}}_\mathrm{i}\}$, $\{\hat{\mathbf{s}}_\mathrm{s}, \hat{\mathbf{p}}_\mathrm{s}, \hat{\mathbf{k}}_\mathrm{s}\}$,$\{\hat{\mathbf{s}}_\mathrm{i}', \hat{\mathbf{p}}_\mathrm{i}', \hat{\mathbf{k}}_\mathrm{i}\}$, and $\{\hat{\mathbf{s}}_\mathrm{s}', \hat{\mathbf{p}}_\mathrm{s}', \hat{\mathbf{k}}_\mathrm{s}\}$, form right-handed orthogonal coordinate systems. We need to know the angle ψ_i that $\hat{\mathbf{s}}_\mathrm{i}'$ and $\hat{\mathbf{p}}_\mathrm{i}'$ are rotated with respect to $\hat{\mathbf{s}}_\mathrm{i}$ and $\hat{\mathbf{p}}_\mathrm{i}$, and the angle ψ_s that $\hat{\mathbf{s}}_\mathrm{s}'$ and $\hat{\mathbf{p}}_\mathrm{s}'$ are rotated with respect to $\hat{\mathbf{s}}_\mathrm{s}$ and $\hat{\mathbf{p}}_\mathrm{s}$. As usual, these angles can be determined by inner products with each other:

$$\cos\psi_\mathrm{i} = \hat{\mathbf{s}}_\mathrm{i} \cdot \hat{\mathbf{s}}_\mathrm{i}' = \frac{-\sin\beta}{\sqrt{\cos^2\beta\,\sin^2\alpha + \sin^2\beta}}, \tag{29}$$

$$\sin\psi_\mathrm{i} = \hat{\mathbf{p}}_\mathrm{i} \cdot \hat{\mathbf{s}}_\mathrm{i}' = \frac{\cos\beta\,\sin\alpha}{\sqrt{\cos^2\beta\sin^2\alpha + \sin^2\beta}}, \tag{30}$$

$$\cos\psi_\mathrm{s} = \hat{\mathbf{s}}_\mathrm{s} \cdot \hat{\mathbf{s}}_\mathrm{s}' = \frac{-2\sqrt{2}\,\sin\beta}{\sqrt{6 - 2\,\cos 2\beta - 2\,\cos 2\,(\alpha-\delta) - \cos 2\,(\alpha-\beta-\delta) - \cos 2\,(\alpha+\beta-\delta)}}, \tag{31}$$

and

$$\sin\psi_{\rm s} = \hat{\mathbf{p}}_{\rm s}\cdot\hat{\mathbf{s}}'_{\rm s} = \frac{-2\sqrt{2}\,\cos\beta\,\sin(\alpha-\delta)}{\sqrt{6-2\,\cos 2\,\beta-2\,\cos 2\,(\alpha-\delta)-\cos 2\,(\alpha-\beta-\delta)-\cos 2\,(\alpha+\beta-\delta)}}. \tag{32}$$

The angles $\psi_{\rm i}$ and $\psi_{\rm s}$ can then be readily computed from

$$\psi_{\rm i} = \arctan(\cos\psi_{\rm i}, \sin\psi_{\rm i}) = \arctan(-\sin\beta, \cos\beta\sin\alpha), \tag{33}$$

and

$$\psi_{\rm s} = \arctan(\cos\psi_{\rm s}, \sin\psi_{\rm s}) = \arctan(\sin\beta, \cos\beta\sin(\alpha-\delta)). \tag{34}$$

Once again, the function $\arctan(x, y)$ is defined by Eq. 13.

The elements of the Mueller matrix BRDF can be determined by rotating the two retarders, following the description of Azzam.[14] Dependent upon the configuration of the polarization optics, this transformation may be applied to actively control the polarization selection during data collection, or to transform the Mueller matrix after data collection.

4. THE INSTRUMENT SIGNATURE

For highly polished samples, the measured BRDF can deviate from the true surface BRDF as a result of scattering in the air within the field of view of the receiver.[12,13] In this section, the Mueller matrix BRDF that one should measure for a perfectly smooth surface in an ambient air environment will be derived and compared with experiment. This contribution to the signal should be subtracted from any measured signal in order to extract a sample-specific BRDF.

The instrument signature $I(\hat{\mathbf{k}}_1, \hat{\mathbf{k}}_2)$, defined as the radiant power normalized by the incident irradiance, under conditions where Raleigh scattering in air dominates is given by,[13]

$$I(\hat{\mathbf{k}}_1, \hat{\mathbf{k}}_2) = I_0 \frac{l_{\rm FOV}}{|\sin\theta_{12}|}|\hat{\sigma}_1\cdot\hat{\sigma}_2|^2, \tag{35}$$

where

$$I_0 = \frac{4\pi^2}{\lambda^4}\frac{(n-1)^2}{N}, \tag{36}$$

n is the index of refraction of air, N is the number density of air, $l_{\rm FOV}$ is the diameter of the field of view at the sample in a direction perpendicular to the viewing direction, and $\hat{\sigma}_1$ and $\hat{\sigma}_2$ are unit vectors in the directions of the electric fields of the incident and scattered beams, respectively. At 20 °C, a wavelength of 532 nm, at standard atmospheric pressure, $I_0 = 1.29\times10^{-6}$ m^{-1}.

Figure 5 shows the various contributions to the instrument signature when the laser strikes a highly reflecting sample. Five paths are shown radiating toward the detector. Path S is the surface-induced radiance intrinsic to the sample. Path 1 is the Rayleigh scatter from the incident beam directed toward the detector without any interaction with the surface. Path 2 is the Rayleigh scatter from the reflected beam, or light which interacts with the surface first, and then with the air. Path 3 is the Rayleigh scatter from the image of the incident beam in the surface, or light which interacts with the air first, then with the surface. Finally, path 4 is the Rayleigh scatter from the image of the reflected beam in the surface, or light which reflects from the surface, scatters from the air, and then reflects from the surface again. Considering the lengths of the paths of light within the field-of-view of the receiver (assumed to be circular and centered on the illuminated spot and underfilling the sample), and the different interactions with the surface outlined above, it can be shown that the equivalent BRDF resulting from Rayleigh scatter in the plane of incidence and for simple polarization states is

$$f_{\rm Rayleigh}(\hat{\mathbf{k}}_{\rm s}) = \frac{1}{2\cos\theta_{\rm s}}\left\{I(\hat{\mathbf{k}}_{\rm i}, \hat{\mathbf{k}}_{\rm s})[1+R(\theta_{\rm i})R(\theta_{\rm s})] + I(\hat{\mathbf{k}}_{\rm r}, \hat{\mathbf{k}}_{\rm s})[R(\theta_{\rm i})+R(\theta_{\rm s})]\right\}, \tag{37}$$

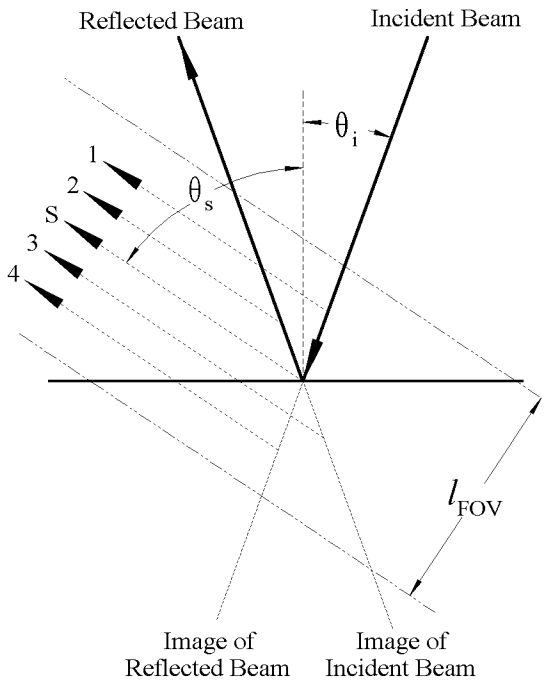

Figure 5 The contributions to the instrument signature.

where $R(\theta)$ is the specular reflectance of the sample at an incident angle of θ, and $\hat{\mathbf{k}}_\mathrm{r}$ is the specular direction.

When viewing the sample out of the plane of incidence, or when using polarization states which are neither purely s- nor p-polarized, the results become more complicated, since the polarizations mix and the different reflection coefficients for the two polarizations must properly be taken into account. The appropriate basis vectors for describing the polarization of the incident and scattered light was derived in Sec. 3.C. The basis vectors for describing the polarization of the specularly scattered incident light can be defined to be

$$\hat{\mathbf{s}}'_\mathrm{ir} = \hat{\mathbf{s}}'_\mathrm{i} \tag{38}$$

and

$$\hat{\mathbf{p}}'_\mathrm{ir} = (-\hat{\mathbf{x}}'\hat{\mathbf{x}}' - \hat{\mathbf{y}}'\hat{\mathbf{y}}' + \hat{\mathbf{z}}'\hat{\mathbf{z}}') \cdot \hat{\mathbf{p}}'_\mathrm{i}, \tag{39}$$

while the basis vectors for describing the light which is specularly reflected into the viewing direction are

$$\hat{\mathbf{s}}'_\mathrm{sr} = \hat{\mathbf{s}}'_\mathrm{s} \tag{40}$$

and

$$\hat{\mathbf{p}}'_\mathrm{sr} = (-\hat{\mathbf{x}}'\hat{\mathbf{x}}' - \hat{\mathbf{y}}'\hat{\mathbf{y}}' + \hat{\mathbf{z}}'\hat{\mathbf{z}}') \cdot \hat{\mathbf{p}}'_\mathrm{s}. \tag{41}$$

The Jones matrices for the geometric factors for the four terms can then be shown to be

$$\begin{aligned} J_1 &= \begin{pmatrix} \hat{\mathbf{s}}'_\mathrm{i} \cdot \hat{\mathbf{s}}'_\mathrm{s} & \hat{\mathbf{s}}'_\mathrm{i} \cdot \hat{\mathbf{p}}'_\mathrm{s} \\ \hat{\mathbf{p}}'_\mathrm{i} \cdot \hat{\mathbf{s}}'_\mathrm{s} & \hat{\mathbf{p}}'_\mathrm{i} \cdot \hat{\mathbf{p}}'_\mathrm{s} \end{pmatrix} \\ &= \begin{pmatrix} -\cos\phi_\mathrm{s} & \cos\theta_\mathrm{i}\sin\phi_\mathrm{s} \\ -\cos\theta_\mathrm{s}\sin\phi_\mathrm{s} & \sin\theta_\mathrm{i}\sin\theta_\mathrm{s} - \cos\theta_\mathrm{s}\cos\theta_\mathrm{i}\cos\phi_\mathrm{s} \end{pmatrix}, \end{aligned} \tag{42}$$

$$\begin{aligned} J_2 &= \begin{pmatrix} r_s(\theta_\mathrm{i})\hat{\mathbf{s}}'_\mathrm{ir} \cdot \hat{\mathbf{s}}'_\mathrm{s} & r_p(\theta_\mathrm{i})\hat{\mathbf{s}}'_\mathrm{ir} \cdot \hat{\mathbf{p}}'_\mathrm{s} \\ r_s(\theta_\mathrm{i})\hat{\mathbf{p}}'_\mathrm{ir} \cdot \hat{\mathbf{s}}'_\mathrm{s} & r_p(\theta_\mathrm{i})\hat{\mathbf{p}}'_\mathrm{ir} \cdot \hat{\mathbf{p}}'_\mathrm{s} \end{pmatrix} \\ &= \begin{pmatrix} -r_s(\theta_\mathrm{i})\cos\phi_\mathrm{s} & r_p(\theta_\mathrm{i})\cos\theta_\mathrm{i}\sin\phi_\mathrm{s} \\ -r_s(\theta_\mathrm{i})\cos\theta_\mathrm{s}\sin\phi_\mathrm{s} & r_p(\theta_\mathrm{i})(-\sin\theta_\mathrm{i}\sin\theta_\mathrm{s} - \cos\theta_\mathrm{s}\cos\theta_\mathrm{i}\cos\phi_\mathrm{s}) \end{pmatrix}, \end{aligned} \tag{43}$$

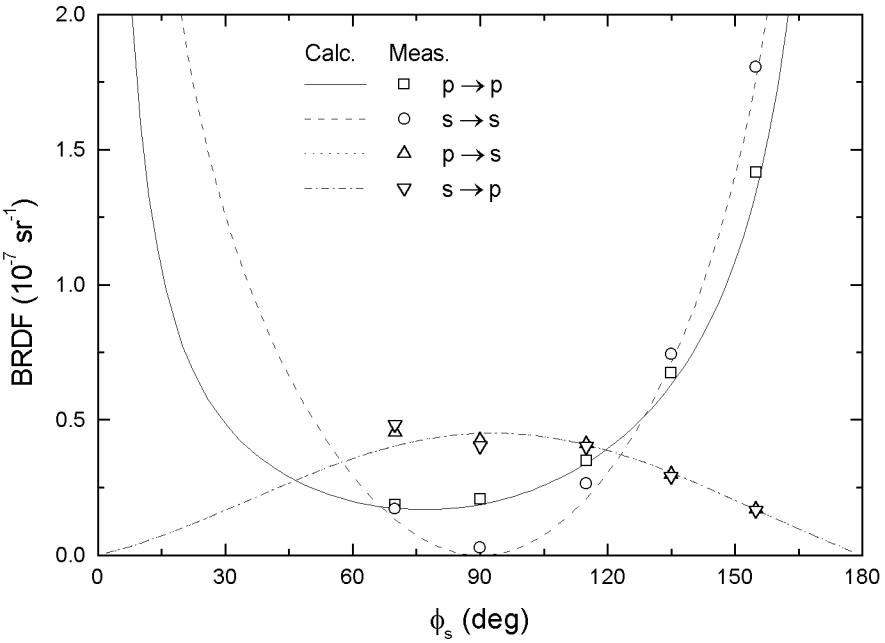

Figure 6 The measured polarized BRDF ($s \to s$, $p \to s$, $s \to p$, and $p \to p$) arising from Rayleigh scatter in the field of view of the receiver. The curves represent the results of calculations described in this paper.

$$
\begin{aligned}
J_3 &= \begin{pmatrix} r_s(\theta_\mathrm{s})\hat{\mathbf{s}}'_\mathrm{i} \cdot \hat{\mathbf{s}}'_\mathrm{sr} & r_s(\theta_\mathrm{s})\hat{\mathbf{s}}'_\mathrm{i} \cdot \hat{\mathbf{p}}'_\mathrm{sr} \\ r_p(\theta_\mathrm{s})\hat{\mathbf{p}}'_\mathrm{i} \cdot \hat{\mathbf{s}}'_\mathrm{sr} & r_p(\theta_\mathrm{s})\hat{\mathbf{p}}'_\mathrm{i} \cdot \hat{\mathbf{p}}'_\mathrm{sr} \end{pmatrix} \\
&= \begin{pmatrix} -r_s(\theta_\mathrm{s})\cos\phi_\mathrm{s} & r_s(\theta_\mathrm{s})\cos\theta_\mathrm{i}\sin\phi_\mathrm{s} \\ -r_p(\theta_\mathrm{s})\cos\theta_\mathrm{s}\sin\phi_\mathrm{s} & r_p(\theta_\mathrm{s})(-\sin\theta_\mathrm{i}\sin\theta_\mathrm{s} - \cos\theta_\mathrm{s}\cos\theta_\mathrm{i}\cos\phi_\mathrm{s}) \end{pmatrix},
\end{aligned}
\tag{44}
$$

and

$$
\begin{aligned}
J_4 &= \begin{pmatrix} r_s(\theta_\mathrm{s})r_s(\theta_\mathrm{i})\hat{\mathbf{s}}'_\mathrm{ir} \cdot \hat{\mathbf{s}}'_\mathrm{sr} & r_s(\theta_\mathrm{s})r_p(\theta_\mathrm{i})\hat{\mathbf{s}}'_\mathrm{ir} \cdot \hat{\mathbf{p}}'_\mathrm{sr} \\ r_p(\theta_\mathrm{s})r_s(\theta_\mathrm{i})\hat{\mathbf{p}}'_\mathrm{ir} \cdot \hat{\mathbf{s}}'_\mathrm{sr} & r_p(\theta_\mathrm{s})r_p(\theta_\mathrm{i})\hat{\mathbf{p}}'_\mathrm{ir} \cdot \hat{\mathbf{p}}'_\mathrm{sr} \end{pmatrix} \\
&= \begin{pmatrix} -r_s(\theta_\mathrm{s})r_s(\theta_\mathrm{i})\cos\phi_\mathrm{s} & r_s(\theta_\mathrm{s})r_p(\theta_\mathrm{i})\cos\theta_\mathrm{i}\sin\phi_\mathrm{s} \\ -r_p(\theta_\mathrm{s})r_s(\theta_\mathrm{i})\cos\theta_\mathrm{s}\sin\phi_\mathrm{s} & r_p(\theta_\mathrm{s})r_p(\theta_\mathrm{i})(\sin\theta_\mathrm{i}\sin\theta_\mathrm{s} - \cos\theta_\mathrm{s}\cos\theta_\mathrm{i}\cos\phi_\mathrm{s}) \end{pmatrix},
\end{aligned}
\tag{45}
$$

respectively. The r_s and r_p are the reflection coefficients for s- and p-polarized light, respectively. Since the phases between all four terms are random, one must sum them in the Mueller representation (i.e. convert to Mueller matrices using algorithms given in van de Hulst[15] or Bohren and Huffman[16]). The out-of-plane equivalent BRDF is then

$$
f_\mathrm{Rayleigh}(\hat{\mathbf{k}}_\mathrm{s}) = \frac{I_0 l_\mathrm{FOV}}{2\cos\theta_\mathrm{s}} \left[\frac{1}{\sin\theta_\mathrm{is}}(M_1 + M_4) + \frac{1}{\sin\theta_\mathrm{rs}}(M_2 + M_3) \right], \tag{46}
$$

where the M_i are the Mueller representations of J_i, and θ_{jk} is the angle subtended by (θ_j, ϕ_j) and (θ_k, ϕ_k) using Eq. 16.

Figure 6 shows the results of a measurement of Rayleigh scattering in the presence of a highly polished silicon wafer. The measurement of the BRDF was carried out with two fields of view ($l_\mathrm{FOV} = 58.1$ mm and 11.5 mm) so that any contribution from the sample, albeit small, could be subtracted. The results are presented as $s \to s$, $p \to p$, $s \to p$, and $p \to s$ polarized BRDFs. The curves shown in Fig. 6 are results of evaluating Eq. 46 with $l_\mathrm{FOV} = 46.6$ mm, and are in good agreement with the measurement.

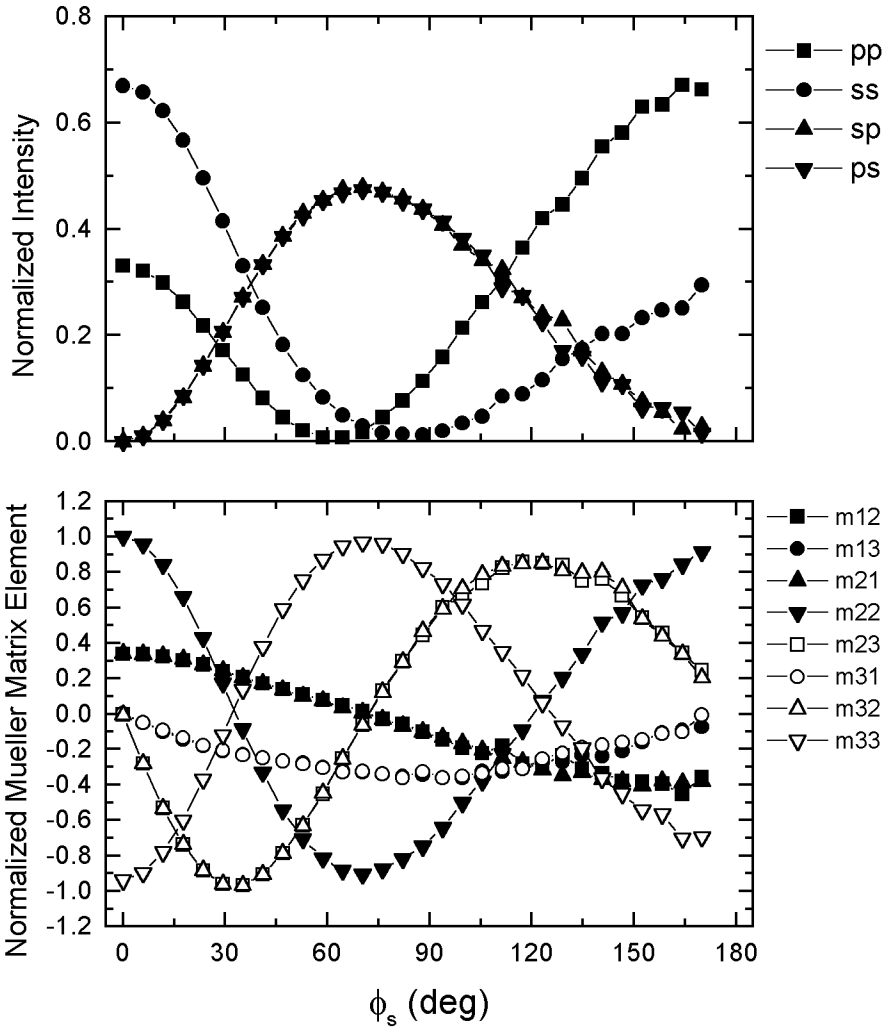

Figure 7 The $p \to p$, $s \to s$, $s \to p$, and $p \to s$ intensities (top) and the non-handed Mueller matrix elements (bottom) for out-of-plane scattering from the rough backside of a silicon wafer. The intensities are normalized by the sum of all four intensities, and the Mueller matrix elements are normalized by the element m_{11}. The incident angle θ_i and scattering angle θ_s were 45°, and the wavelength was 532 nm.

5. RESULTS AND DISCUSSION

A series of consecutive measurements of the Mueller matrix with no sample present should yield the unity matrix and an estimate of random and systematic uncertainties in Mueller matrix measurements. Such a measurement was carried out with eighty measurements and yielded

$$\begin{pmatrix} 1 & (5.2 \pm 1.7) \times 10^{-4} & (1.6 \pm 0.7) \times 10^{-4} & - \\ (8.1 \pm 0.9) \times 10^{-4} & 0.9995 \pm 0.0001 & (4.0 \pm 0.9) \times 10^{-4} & - \\ (-4.2 \pm 1.7) \times 10^{-4} & (2.2 \pm 0.3) \times 10^{-3} & 1.0008 \pm 0.0001 & - \\ - & - & - & - \end{pmatrix}.$$

The uncertainties quoted above are the standard deviation of the eighty measurements, and therefore are an indication of the random uncertainty for a single measurement. The deviation of this matrix from the unity matrix is an indication of systematic errors in the system. No systematic drift in the values was observed.

Figure 7 shows results of Mueller matrix measurements from the rough backside of a silicon wafer. Since the retardations were both $\lambda/2$, only the 3×3 non-handed matrix elements were measured. The results demonstrate that even a surface as rough as the backside of a silicon wafer has structure in the Mueller matrix that should lead to information about the scattering mechanisms. In fact, it can be shown that the data in Fig. 7 exhibits excellent agreement with an incoherent sum of Rayleigh-Rice theory[1,17,18] with a completely depolarizing contribution. An understanding of the scattering from these rough surfaces should enable enhanced detection of particles and defects on these materials, as well as improved emissivity models necessary for radiant thermometry during rapid thermal processing. Further discussion of these data is beyond the scope of this paper and will be presented elsewhere.

REFERENCES

[1] J. C. Stover, *Optical Scattering: Measurement and Analysis*, (McGraw-Hill, New York, 1990).

[2] E. R. Méndez, A. G. Navarrete, and R. E. Luna, "Statistics of the polarization properties of one-dimensional randomly rough surfaces," J. Opt. Soc. Am. A **12**, 2507–16 (1995).

[3] D. L. Jordan, G. D. Lewis, and E. Jakeman, "Emission polarization of roughened glass and aluminum surfaces," Appl. Opt. **35**, 3583–90 (1996).

[4] S.-M. F. Nee, "Polarization of specular reflection and near-specular scattering by a rough surface," Appl. Opt. **35**, 3570–82 (1996).

[5] T. A. Germer, "Angular dependence and polarization of out-of-plane optical scattering from particulate contamination, subsurface defects, and surface microroughness," (submitted for publication.).

[6] T. A. Germer, C. C. Asmail, and B. W. Scheer, "The polarization of out-of-plane scattering from microrough silicon," (submitted for publication.).

[7] R. E. Luna, "Scattering by one-dimensional random rough metallic surfaces in a conical configuration: several polarizations," Opt. Lett. **21**, 1418–20 (1996).

[8] W. S. Bickel, R. R. Zito, and V. Iafelice, "Polarized Light Scattering From Metal Surfaces," J. Appl. Phys. **61**, 5392 (1987).

[9] V. J. Iafelice, and W. S. Bickel, "Polarized Light-Scattering Matrix Elements for Select Perfect and Perturbed Optical Surfaces," Appl. Opt. **26**, 2410–5 (1987).

[10] G. Videen, J.-Y. Hsu, W. S. Bickel, and W. L. Wolfe, "Polarized light scattered from rough surfaces," J. Opt. Soc. Am. A **9**, 1111-8 (1992).

[11] E. Bahar, and M. A. Fitzwater, "Like- and cross-polarized cross sections for random rough surfaces: theory and experiment," J. Opt. Soc. Am. A **2**, 2295–303 (1985).

[12] C. C. Asmail, C. L. Cromer, J. E. Proctor, and J. J. Hsia, "Instrumentation at the National Institute of Standards and Technology for bidirectional reflectance distribution function (BRDF) measurements," Proc. SPIE **2260**, 52–61 (1994).

[13] C. Asmail, J. Hsia, A. Parr, and J. Hoeft, "Rayleigh scattering limits for low-level bidirectional reflectance distribution function measurements," Appl. Opt. **33**, 6084-91 (1994).

[14] R. M. A. Azzam, "Photopolarimetric measurement of the Mueller matrix by Fourier analysis of a single detected signal," Opt. Lett. **2**, 148 (1978).

[15] H. C. v. d. Hulst, *Light Scattering by Small Particles*, (Dover, New York, 1981).

[16] C. F. Bohren, and D. R. Huffman, *Absorption and Scattering of Light by Small Particles*, (Wiley, New York, 1983).

[17] S. O. Rice, "Reflection of Electromagnetic Waves from Slightly Rough Surfaces," Comm. Pure and Appl. Math. **4**, 351–78 (1951).

[18] D. E. Barrick, *Radar Cross Section Handbook*, (Plenum, New York, 1970).